BMC Gastroenterology

RESEARCH

Open Access

Deep learning-based CT radiomics predicts prognosis of unresectable hepatocellular carcinoma treated with TACE-HAIC combined with PD-1 inhibitors and tyrosine kinase inhibitors

Linan Yin[1], Ruibao Liu[1*], Wei Li[2], Shijie Li[1] and Xunbo Hou[1]

Abstract

Objective To develop and validate a computed tomography (CT)-based deep learning radiomics model to predict treatment response and progression-free survival (PFS) in patients with unresectable hepatocellular carcinoma (uHCC) treated with transarterial chemoembolization (TACE)-hepatic arterial infusion chemotherapy (HAIC) combined with PD-1 inhibitors and tyrosine kinase inhibitors (TKIs).

Methods This retrospective study included 172 patients with uHCC who underwent combination therapy of TACE-HAIC with TKIs and PD-1 inhibitors. Among them, 122 were from the Interventional Department of the Harbin Medical University Cancer Hospital, with 92 randomly assigned to the training cohort and 30 cases randomly assigned to the testing cohort. The remaining 50 cases were from the Interventional Department of the Affiliated Fourth Hospital of Harbin Medical University and were used for external validation. All patients underwent liver enhanced CT examination before treatment. Residual convolutional neural network (ResNet) technology was used to extract image features. A predictive model for treatment response of combination therapy and PFS was established based on image features and clinical features. Model effectiveness was evaluated using metrics such as the area under the receiver operating characteristic (ROC) curve (AUC), concordance index (C-index), accuracy, precision, and F1-score.

Results All patients had a median follow-up of 25.2 months (95% CI 24.4–26.0), with a median PFS of 14.0 months (95% CI 8.5–19.4) and a median overall survival (OS) of 26.2 months (95% CI 15.9–36.4) achieved. Objective response rate (ORR) and disease control rate (DCR) was 41.0% and 55.7%, respectively. In the treatment response prediction model, the AUC for the training cohort reached 0.96, with an accuracy of 89.5%, precision of 85.6%, and F1-score of 0.896; the AUC for the testing cohort was 0.87, with an accuracy of 80.4%, precision of 74.5%, and F1-score of 0.802. The AUC of the external validation cohort was 0.85, with accuracy of 79.1%, precision of 73.6%, and f1-score of 0.784. In the PFS prediction model, the predicted AUC for 12 months, 18 months, and 24 months-PFS in the training

*Correspondence:
Ruibao Liu
Liu_ruibao@sina.com

Full list of author information is available at the end of the article

cohort were 0.874, 0.809, 0.801, respectively. The AUC of testing cohort were 0.762, 0.804, 0.792. The AUC of external validation cohort were 0.764, 0.796, 0.773. The C-index of the combination model, radiomics model, and clinical model were 0.75, 0.591, and 0.655, respectively. The calibration curve demonstrated that the combination model was significantly superior to both the radiomics and clinical models.

Conclusions The study provides a CT-based radiomics model that can predict PFS for patients with uHCC treated with TACE-HAIC combined with PD-1 and TKIs.

Keywords Deep learning model, Radiomics, Prognosis, Unresectable liver cancer

Introduction

Hepatocellular carcinoma (HCC) represents the most common malignant tumor worldwide, characterized by poor prognosis and limited treatment options, especially for patients with unresectable HCC (uHCC) [1–3]. According to the Barcelona Clinic Liver Cancer (BCLC) staging guidelines, transarterial chemoembolization (TACE) serves as standard treatment modality for intermediate-stage HCC and is widely utilized in the treatment of uHCC in some countries [4]. Recently, the combination of TACE and HAIC has emerged as a significant therapeutic approach for patients with uHCC, markedly improving survival rates. Studies have demonstrated that the combination of TACE and HAIC has better therapeutic effects on unresectable HCC [5, 6]. TACE-HAIC can effectively manage HCC; however, its overall efficacy is often compromised by tumor recurrence and metastasis. Ischemia and hypoxia caused by embolism and tumor necrosis may lead to an increase in vascular endothelial growth factor (VEGF) and angiogenesis, which enhances the likelihood of tumor recurrence and metastasis. The treatment landscape for HCC has recently transitioned to include immunotherapy combinations, with PD-1 inhibitors and tyrosine kinase inhibitors (TKIs) demonstrating potential synergistic effects when combined with TACE-HAIC [7–9]. However, due to HCC's high heterogeneity and the absence of precise biomarkers for predicting therapeutic efficacy, considerable variability exists in the effectiveness of these combination treatments. Consequently, there is currently no accurate and effective method to screen patients who may benefit from these combination therapies.

Recently, radiomics has demonstrated great potential in the diagnosis of liver diseases, analyzing tumor biological characteristics, and evaluating prognosis by converting medical images into quantitative data [10–12]. Due to its high spatial resolution and rapid imaging capabilities, computed tomography (CT) is frequently employed in radiomics research [13]. Studies have indicated that the preoperative use of CT radiomics features, when combined with clinical features, exhibits excellent performance in predicting the efficacy of TACE in patients with HCC. The area under the curve (AUC) of the prediction model in the internal and external validation groups was 0.94 and 0.90, respectively [14]. Preoperative CT imaging omics characteristics can accurately predict the efficacy and overall survival (OS) of HAIC for advanced unresectable colorectal cancer with liver metastasis [15]. Moreover, similar studies have been reported on prognosis prediction in surgical resection [16], immunotherapy [17], and targeted therapy [18, 19], thereby providing a feasible evaluation tool for patients before treatment. However, thus far, no studies focusing on the additional benefits and prognosis prediction of CT radiomics features in TACE-HAIC combined with PD-1 inhibitors and TKIs have yet been published.

This study seeks to develop a deep learning model based on clinical and radiomics features to predict the efficacy of TACE-HAIC combined with PD-1 inhibitors and TKIs for treating unresectable HCC, aiming to enhance the accuracy of comprehensive treatment prediction and optimize patient management and prognosis.

Materials and methods

Study population

This retrospective study was approved by the Ethics Committee of Harbin Medical University Cancer Hospital (Ethics Number: 2023-281-IIT). Patients with unresectable HCC treated with TACE-HAIC and TKIs and PD-1 inhibitor treatment at the Harbin Medical University Cancer Hospital and Affiliated Fourth Hospital of Harbin Medical University between January 2020 to December 2022 were included. The diagnosis of HCC was based on the clinical or pathological diagnostic criteria in the Chinese Guidelines for the Diagnosis and Treatment of Primary Liver Cancer [20].

The inclusion criteria were as follows: (1) HCC confirmed by pathology or clinical examination in two hospitals from January 2020 to December 2022; (2) had neither received previous treatment nor were suitable for radical surgery, transplantation, or radical ablation; (3) aged > 18 years; (4) an Eastern Cooperative Oncology Group (ECOG) score of 0 or 1 and Child–Pugh grade of A or B; (5) lesions with imaging reproducibility; and (6) complete raw data from enhanced CT scans were obtainable within 7 days prior to treatment. Exclusion criteria included: (1) abnormal liver and kidney function and coagulation function that cannot be corrected;

(2) had clear contraindications for the use of TKIs and PD-1 inhibitors in cases of uncorrectable cardiopulmonary dysfunction; (3) clear contraindications for TACE and HAIC; and (4) expected survival time of < 3 months (supplemental Fig. 1).

Clinical information for patients prior to treatment was retrospectively collected, including age, gender, hepatitis status, cirrhosis, Child–Pugh grading, ECOG score, maximum tumor diameter, number of tumors, presence of capsule, diffuse distribution, vascular invasion (portal vein tumor thrombus, hepatic vein, and inferior vena cava invasion), extrahepatic metastasis, lymph node metastasis, CNLC staging, BCLC staging, and AFP level.

Treatment process

TACE-HAIC: TACE treatments utilized the femoral artery approach. A super selective intubation technique was employed for embolization, with a mixture of iodized oil (5–20 mL) and pirarubicin (40–60 mg) as the embolic agent. Appropriate embolization was necessary to achieve incomplete devascularization for tumors with a single blood supply. For tumors supplied by multiple blood vessels, conventional embolization or complete devascularization was performed on blood vessels with a lower tumor load, and appropriate embolization was performed on blood vessels with a higher tumor load. After embolization, a catheter was placed at the beginning of the tumor blood supply vessel for HAIC, which is performed following TACE. After 2–3 treatment cycles, once imaging tests show the tumor lacks significant activity and hematological indicators like AFP and abnormal thrombin levels normalize, TACE treatment ceases, and TKI and PD-1 inhibitor therapy proceeds. The mFOLFOX regimen containing oxaliplatin as the chemotherapy regimen was selected. The mFOLFOX regimen comprised arterial infusion of oxaliplatin 85 mg/m^2 for 2 h, calcium folinate 400 mg/m^2 for 1 h, fluorouracil 400 mg/m^2 for arterial infusion, and continuous arterial infusion of 2,400 mg/m^2 for 46 h. Dosage adjustments will be based on the number of treatments, laboratory test outcomes, and clinical signs. The abovementioned operation should be repeated every 3–4 weeks. The median number of treatment sessions in this study was 3 ± 1 days.

TKIs and PD-1 inhibitors: The TKIs used in this study included oral administration of donafenib 0.2 g twice daily; lenvatinib 8 mg (body weight ≤ 60 kg)/12 mg (body weight > 60 kg) orally administered once daily; and sorafenib 0.4 g orally administered twice daily. The ICIs used in this study included camrelizumab, sintilimab, and tislelizumab which were all intravenously administered at a dose of 200 mg every 21 days. Systemic treatment was suspended during intervention therapy. Consider dose reduction, temporary discontinuation of medication, or switching to second-line agents in cases of intolerable toxic side effects or confirmed disease progression.

Follow-up and outcomes

Follow-up assessments were conducted every 6 to 9 weeks after the combination therapy, including radiological examinations (enhanced CT or MRI scan of the abdomen and plain CT scan of the chest and abdomen) and laboratory examinations. Two radiologists with senior professional titles reviewed all collected imaging data, and the efficacy of the treated tumors was evaluated according to the Modified Response Evaluation Criteria in Solid Tumors (mRECIST). Efficacy was evaluated using objective response (OR), no response (NR), complete response (CR), partial response (PR), disease stability (SD), and disease progression (PD). OR was defined as complete response and partial response (CR + PR). NR was defined as disease stability and disease progression (SD + PD). An inconsistent efficacy evaluation was resolved through consultation between radiologists and clinical doctors. The date of the last follow-up was October 1, 2023. The assessment of Treatment-Related Adverse Events (TRAEs) is conducted based on the Common Terminology Criteria for Adverse Events (CTCAE), Version 5.0.

Image acquisition and imaging processing

The enhanced CT images of the liver were obtained from the Picture Archival and Communication System of Harbin Medical University Cancer Hospital and Affiliated Fourth Hospital of Harbin Medical University. All patients underwent GE (Optima) 64-slice spiral CT or Siemens (SOMATOM Definition Flash) dual-source spiral CT.

The CT raw DICOM format files of the 122 patients from the Harbin Medical University Cancer Hospital were imported into 3D Slicer software (version: 5.5.0, https://www.slicer.org/). Two experienced imaging experts, one with 10 years of experience and the other with 20 years of experience, will independently identify the regions of interest of all tumors. When there were significant differences in the regions of interest drawn by the two, they negotiated to resolve the disagreement. If the disagreement could not be resolved, the region of interest identified by the senior expert prevailed. To determine the region of interest (ROI) of the tumor, two experienced radiologists determined the entire sequence of the CT images (including 2,991 HCC slices). All conflicting opinions were resolved through negotiation, and the resulting ROI included the complete tumor and surrounding tissue.

In the Python 3.9 environment, the dicom2nifti library converted DICOM files into NIfTI format. Following this, the SimpleITK library was employed to process the NIfTI

files and extract imaging slices. After filtering out slices without a region of interest (ROI), the dataset retained consisted of 2,991 valid slices. Each slice was linked to a unique DICOM image ID, which was then matched with corresponding clinical data, enabling the construction of a dataset suitable for the ResNet50 + MLP network architecture. Fine-tuning this structure on the dataset allowed for the determination of optimal model weights. Each slice associated with the same ID was input into this structure, and the output from the final layer on the left channel, representing the extracted image features, was averaged across slices to obtain the imaging features for that specific ID.

Construction and evaluation of the ResNet50 + MLP model

In traditional convolutional neural network (CNN) structures, as the number of layers increases, gradient vanishing and exploding problems become more severe, which limits the depth design of CNN. Residual CNN (ResNet) introduces residual learning, which enables the network to achieve identity mapping deeply through skip connections and shortcuts, effectively solving the problems of vanishing and exploding gradients. Skip connections allow a portion of gradients to bypass the nonlinear layer during backpropagation and propagate directly, thereby making network training faster and more effective. Given its superior feature extraction capability and efficient performance, ResNet has been widely used in image classification, object detection, and image segmentation. This study was based on ResNet50 and used two input channels (images and clinical features) for predicting the efficacy of tumor treatment according to the mRECIST evaluation criteria. The model structure is shown in Fig. 1.

To improve the fitting speed of the model and address the scarcity of CT image data, transfer learning was used to handle imbalanced datasets and sparse sample learning problems. Model performance and generalization ability are enhanced by pretraining on the ImageNet database. ImageNet has 14 million images and thousands of categories, making transfer learning an extremely effective tool when resources are limited. To better meet our needs, we froze the first 49-layer parameters of ResNet50 in the pre-trained network, which can significantly improve the training speed of the network model. An additional multilayer perceptron (MLP) layer was added. Using MLP to reduce the dimensionality of feature maps from ResNet50 and to extract abstract features through multiple hidden layers identifies the most significant information in the image. At the end of the network, the filtered image features are concatenated with clinical features, and the task is classified using a fully connected layer. During the training process, the Adaptive Moment Estimation (Adam) algorithm optimizes the weights of

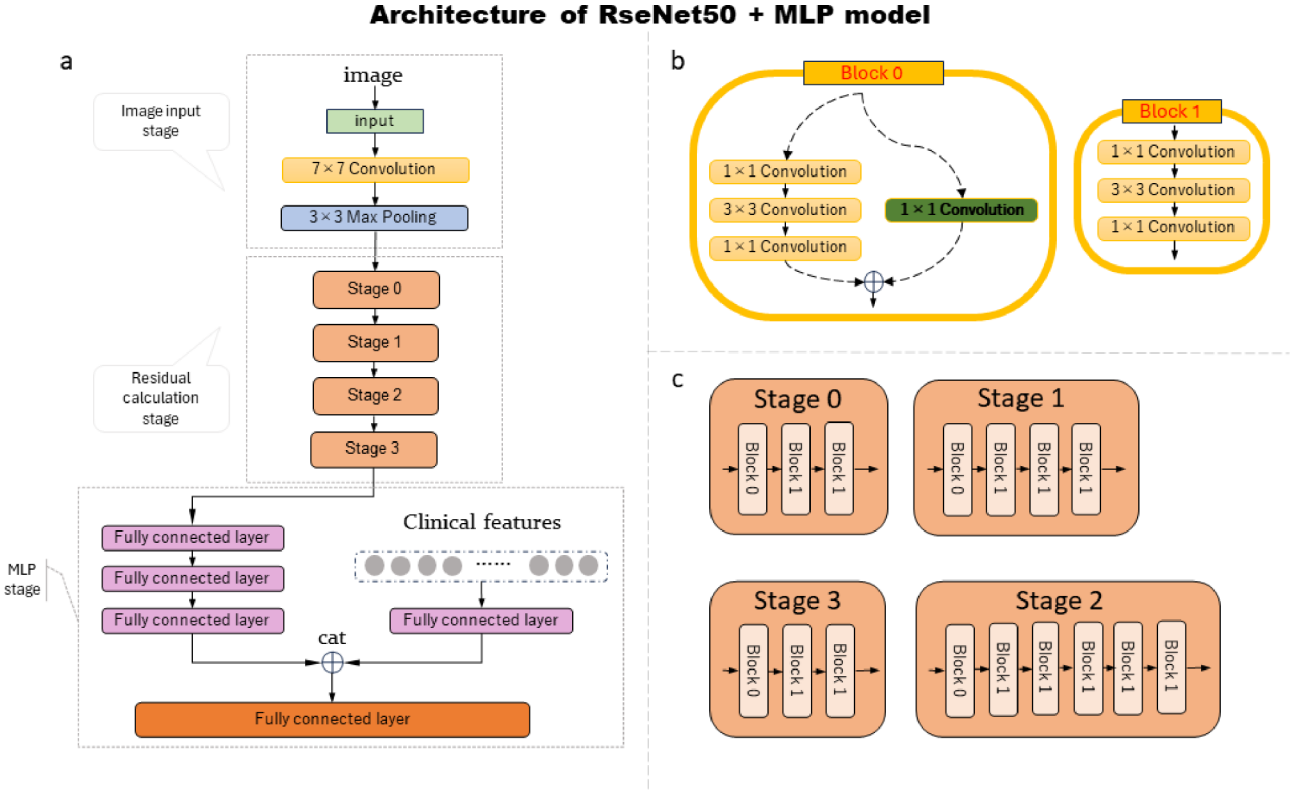

Fig. 1 Architecture of RseNet50 + MLP model

the network parameters. The Adam algorithm combines the momentum algorithm and the RMSprop algorithm, which has better stability in complex and convex optimization problems. By fine-tuning the parameters, the learning rate is set to 1e-5, and to ensure that the model can fully cover the data and achieve efficient training, the number of epochs is 100. The loss function employs binary cross-entropy loss and ultimately calculates the classification probability of the output layer using the SoftMax function on the model's output. Choose AUC and accuracy to evaluate model performance. Among 172 patients, 122 had CT data divided into training and testing cohorts in a 3:1 ratio, with the other 50 serving as external validation cohort. The training loss of the model and the ROC curves of the training, testing and external validation cohort were shown in Fig. 2.

Construction of the nomogram for PFS

Compared with the extensive range of radiomics features extractable from medical imaging data including shape features, first-order statistical features, texture features, and high-order statistical features, the feature extraction and filtering capabilities of the ResNet50 + MLP model prove more suitable for our study. On the one hand, it eliminates the need for extensive analysis and filtering of radiomics features. On the other hand, residual structures effectively associate shallow features with deep features, and the MLP algorithm more effectively filters out the best abstract features (Fig. 3).

First, the image feature extraction module, representing the encoding stage in ResNet50 + MLP, is loaded. The corresponding feature image is obtained after inputting the sliced image into the feature extraction module. Subsequently, it is combined with the processed clinical features and the results in Resnet50 + MLP (the classification probability of mRECIST) to form a covariate. Multivariate Cox regression analyzed covariates and ultimately determined the variables required to construct the model.

The Kaplan-Meier curve evaluated PFS, and Cox regression analyzed the univariate analysis of all clinical features. The risk factors affecting patient survival were analyzed using Cox regression. To draw nomograms for predicting patient prognosis, the RMS software package of the R language (version: 4.3.1, https://www.r-project.org/) was used.

Statistical analysis

Statistical analysis was conducted using Statistical Package for the Social Sciences (version 29, IBM, Armonk, NY, USA) and Python v3.11.5 software. The sample size estimation was performed using PASS 15 software and involved a single-sample log-rank test. To determine whether data conformed to a normal distribution, the Kolmogorov–Smirnov test was utilized; quantitative data were expressed as means ± standard deviation (SD). Quantitative data comparisons were made using the independent sample t-test or Mann–Whitney U-test. Counting data comparisons utilized the chi-square test. Univariate and multivariate Cox regression analyses were employed to screen for clinical variables and establish regression models. The Kaplan–Meier method was utilized to plot the survival curve. The prediction of treatment response relied on the AUC, and the accuracy, precision, and F-1 score were utilized to evaluate the effectiveness of the model. For the PFS prediction model, performance evaluation utilized the ROC curve and C-index (consistency index). Bilateral $P < 0.05$ was indicative of a statistically significant difference.

Results

Clinical characteristics of the patients

A total of 122 HCC patients participated in the study, comprising 92 in the training set and 30 in the internal testing set (Supplemental Fig. 1). No significant differences were observed in clinical characteristics between the training set and the internal testing set. Of these patients, 104 (85.2%) and 18 (14.8%) were male and female patients, respectively, with a median age of 54 ± 10.2 years. Of the patients, 82 (67.2%) had cirrhosis. Hepatitis B patients comprised 76.2%, hepatitis C patients comprised 7.4%, and non-hepatitis patients

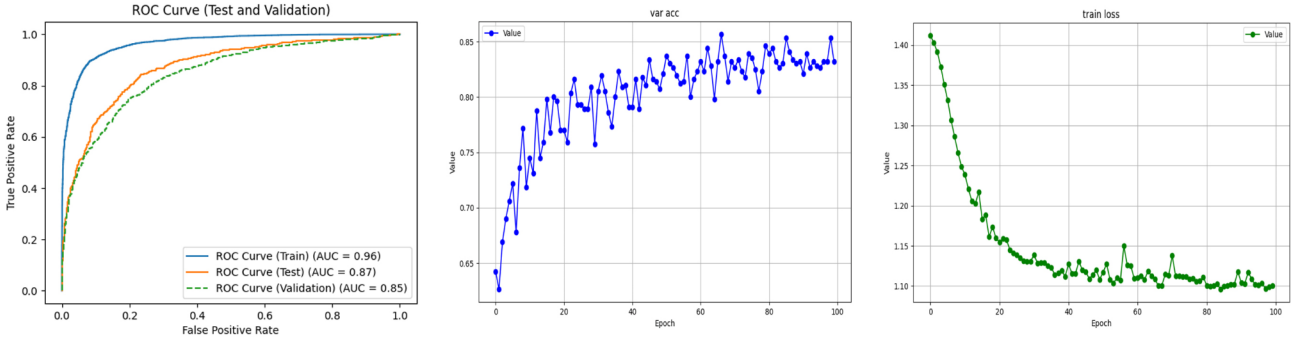

Fig. 2 The ROC curves of the training, testing and external validation cohort

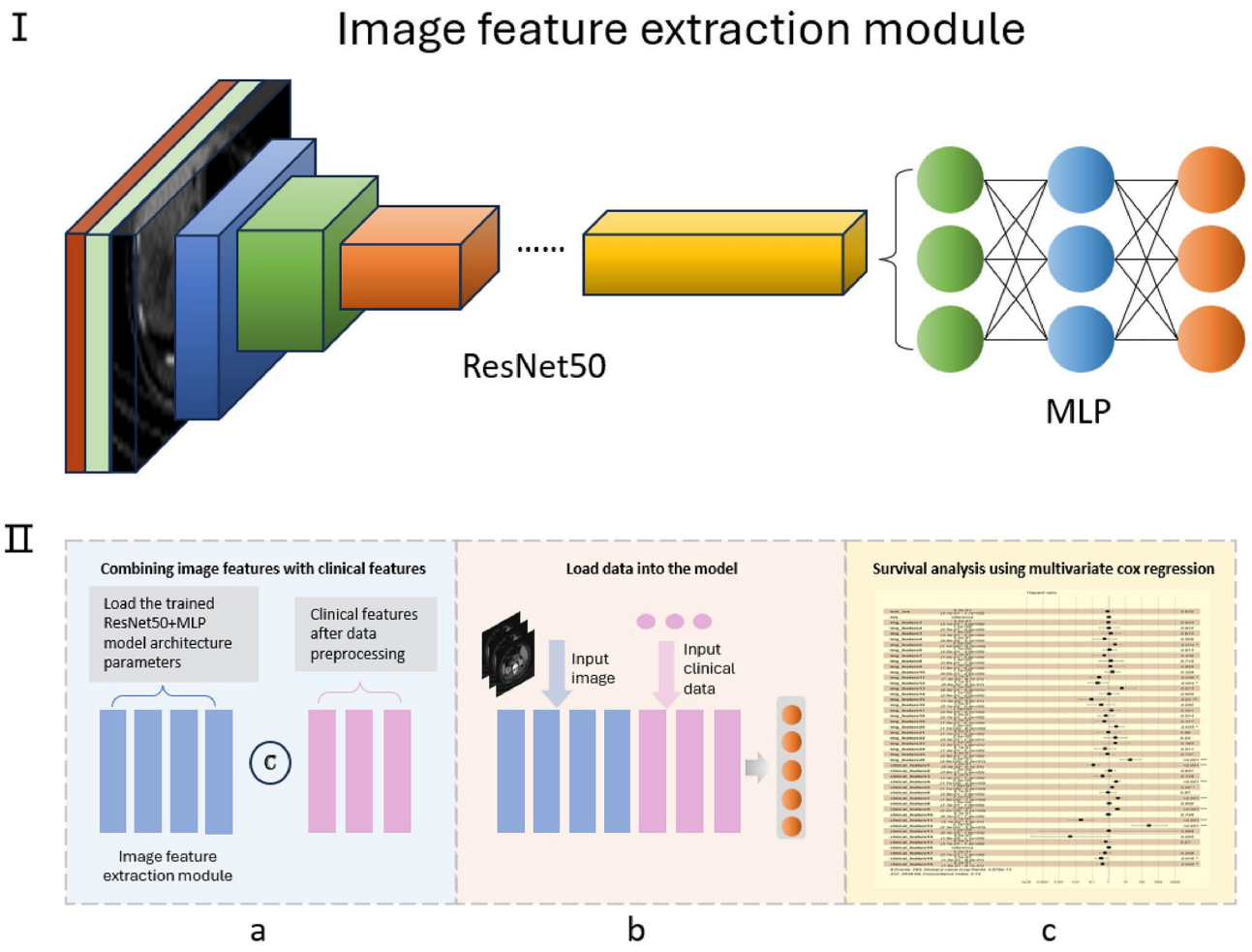

Fig. 3 Image feature extraction module

comprised 16.4%. Moreover, 105 (86.1%) cases of Child–Pugh grade A were recorded, including 61 (50.0%) and 44 (36.1%) cases of A5 and A6, respectively, and 17 (13.9%) cases presented Child–Pugh grade B. Other clinical features are shown in Table 1.

The median follow-up time was 25.2 (95% confidence interval [CI]: 24.4–26.0) months, with a median PFS of 14.0 (95% CI: 8.5–19.4) months and a median OS of 26.2 (95% CI: 15.9–36.4) months (Supplemental Fig. 2). Following treatment, 12 (9.8%) patients achieved CR, 38 (31.1%) achieved PR, 18 (14.8%) achieved SD, and 54 (44.3%) achieved PD. In addition, 54 patients remained alive during the most recent follow-up. The cumulative 12-, 18-, 24-, and 30-month OS rates were 77.0%, 59.8%, 35.2%, and 18.0%, respectively. The 6-, 12-, 18-, 24-, and 30-month PFS rates were 91.0%, 62.3%, 52.5%, 32.0%, and 15.6%, respectively. The overall ORR was 41.0%, and the overall DCR was 55.7%. Among all enrolled cases, the incidence rate of treatment-related adverse events of any grade was 100%, with a 19.7% (24/122) incidence rate of grade 3–4 treatment-related adverse events. No grade 5 adverse events occurred are shown in supplemental Table 1.

Predictive performance of deep learning models for treatment response

The CT data of all enrolled patients were randomly divided into a training group and a testing group at a ratio of 3:1. Changes in training loss and the ROC curves of the training and validation sets are depicted in Fig. 2. A clinical-radiomics multimodal model was constructed using five selected clinical features and radiomics features extracted by ResNet50 + MLP. The model was employed to predict the treatment response to combination therapy based on mRECIST. The AUC of the model in the training cohort reached 0.96, with an accuracy of 89.5%, a precision of 85.6%, and an F-1 score of 0.896. The AUC of the model in the testing cohort was 0.87, with an accuracy of 80.4%, precision of 74.5%, and an F-1 score of 0.802. The AUC of the model in the external validation cohort reached 0.85, with an accuracy of 79.1%, a precision of 73.6%, and an F-1 score of 0.784 (Fig. 4).

Table 1 Baseline characteristics of patients in training cohort, testing cohort, and validation cohort

Characteristics	Total (*N* = 122)	Training cohort (*N* = 92)	Testing cohort (*N* = 30)	*P* value	Validation cohort (*N* = 50)
Age, (years), mean (SD)	54.0 (10.2)	53.9 (10.7)	54.5 (8.7)	0.773	58.8 (10.6)
Sex, No. (%)				1.000	
Female	18 (14.8)	14 (15.2)	4 (13.3)		4 (8.0)
Male	104 (85.2)	78 (84.8)	26 (86.7)		46 (92.0)
CNLC Stage, No. (%)				0.093	
IIa	14 (11.5)	8 (8.7)	6 (20.0)		0 (0.0)
IIb	25 (20.5)	23 (25.0)	2 (6.7)		0 (0.0)
IIIa	35 (28.7)	26 (28.3)	9 (30.0)		38 (76.0)
IIIb	48 (39.3)	35 (38.0)	13 (43.3)		12 (24.0)
BCLC Stage, No. (%)				0.623	
B	39 (32.0)	31 (33.7)	8 (26.7)		0 (0.0)
C	83 (68.0)	61 (66.3)	22 (73.3)		50 (100.0)
Hepatitis, No. (%)				0.549	
No	20 (16.4)	14 (15.2)	6 (20.0)		7 (14.0)
Hepatitis B	93 (76.2)	70 (76.1)	23 (76.7)		38 (76.0)
Hepatitis C	9 (7.4)	8 (8.7)	1 (3.3)		5 (10.0)
Child Pugh Score, No. (%)				0.872	
A5	61 (50.0)	45 (48.9)	16 (53.3)		17 (34.0)
A6	44 (36.1)	34 (37.0)	10 (33.3)		19 (38.0)
B7	16 (13.1)	12 (13.0)	4 (13.3)		10 (20.0)
B8	1 (0.8)	1 (1.1)	0 (0.0)		4 (8.0)
Largest Tumor Diameter (mm), mean (SD)	95.4 (38.1)	93.8 (38.0)	99.2 (41.1)	0.508	116.2 (48.3)
Number of Tumors, No. (%)				0.814	
< 5	73 (59.8)	54 (58.7)	19 (63.3)		31 (62.0)
≥ 5	49 (40.2)	38 (41.3)	11 (36.7)		19 (38.0)
Tumor in One Lobe, No. (%)	69 (56.6)	54 (58.7)	15 (50.0)	0.534	24 (48.0)
Encapsulation, No. (%)	25 (20.5)	17 (18.5)	8 (26.7)	0.481	20 (40.0)
Diffuse Type, No. (%)	44 (36.1)	34 (37.0)	10 (33.3)	0.889	16 (32.0)
Portal Vein Tumor Thrombus, No. (%)	51 (41.8)	36 (39.1)	15 (50.0)	0.404	50 (100.0)
VP, No. (%)				0.096	
VP3	35 (28.7)	22 (23.9)	13 (43.3)		41 (82.0)
VP4	16 (13.1)	14 (15.2)	2 (6.7)		9 (18.0)
Hepatic Vein Cancer Thrombus, No. (%)	6 (4.9)	5 (5.4)	1 (3.3)	1.000	0 (0.0)
Abdominal Lymph Node Metastasis, No. (%)	18 (14.8)	13 (14.1)	5 (16.7)	0.965	5 (10.0)
Extrahepatic Metastasis, No. (%)	39 (32.0)	28 (30.4)	11 (36.7)	0.682	15 (30.0)
Cirrhosis, No. (%)	82 (67.2)	63 (68.5)	19 (63.3)	0.766	48 (96.0)
mRECIST, No. (%)				0.231	
CR	12 (9.8)	10 (10.9)	2 (6.7)		7 (14.0)
PR	38 (31.1)	28 (30.4)	10 (33.3)		5 (10.0)
SD	18 (14.8)	15 (16.3)	3 (10.0)		30 (60.0)
PD	54 (44.3)	39 (42.4)	15 (50.0)		8 (16.0)

mRECIST evaluation was performed every 6 to 9 weeks after combination therapy

Construction of a nomogram and predictive performance of for PFS

Cox regression analysis showed that five clinical features such as AFP level ≥ 400 ng/mL, VP4 type portal vein tumor thrombus, tumor diameter > 10 cm, presence of capsule, and diffuse tumor type and six imaging features, significantly correlated with PFS in patients with HCC (Supplemental Fig. 3). A predictive model for PFS was constructed using clinical features. The predicted AUCs for 12-, 18-, and 24-month PFS in the training cohort were 0.854, 0.797, and 0.803, respectively. The AUC values for the testing cohort were 0.757, 0.675, and 0.69, respectively. The AUC values for the external validation cohort were 0.755, 0.663, and 0.696, respectively. The radiomics model constructed from seven radiomics features had AUCs of 0.765, 0.793, and 0.774 for 12-, 18-, and 24-month PFS in the training cohort, respectively. The AUC of the testing cohort were 0.763, 0.754,

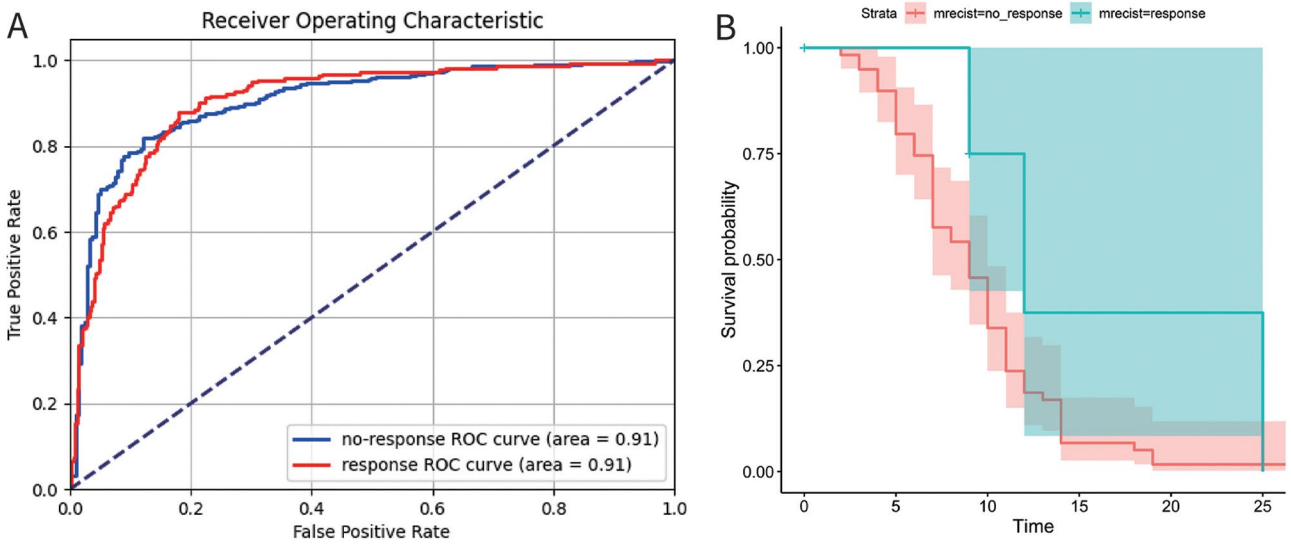

Fig. 4 Predictive performance of clinical-radiomics multimodal model using five clinical features selected and radiomics features

and 0.763, respectively. The AUC of the external validation cohort were 0.733, 0.754, and 0.763, respectively. In the training cohort, the predictive AUCs of the clinical–radiomics multimodal model for 12-, 18-, and 24-month PFS were 0.874 and 0.809 and 0.801, respectively. The AUC of the testing cohort were 0.762, 0.804, and 0.792, respectively. The AUC of the external validation cohort were 0.764, 0.796, and 0.773, respectively. The ROC and calibration curves of the aforementioned three models are displayed in Figs. 5 and 6. The C-indices of the clinical–radiomics multimodal model, radiomics model, and clinical model were 0.75, 0.591, and 0.655, respectively. The calibration curve demonstrated that the performance of the clinical–radiomics multimodal model was significantly superior to that of the other two models. Based on the selected clinical and radiomic features, a nomogram was constructed for predicting PFS following combination therapy, as illustrated in Fig. 7.

Discussion

In this study, a clinical-radiomic (C-R) model was developed and validated based on deep learning, utilizing retrospective data from 172 patients with unresectable HCC treated at Harbin Medical University Cancer Hospital and Affiliated Fourth Hospital of Harbin Medical University. The model predicts treatment response and PFS in patients undergoing treatment with a combination of TACE-HAIC, PD-1 inhibitors, and TKIs. The treatment response predicted by our C-R model was identified as an independent prognostic factor for OS. The C-R model accurately categorize patients with uHCC into treatment-responsive and non-responsive groups based on post-treatment response. Patients predicted by the model to have objective reactions are recommended to receive the combination therapy. Conversely, for patients predicted to be non-responsive, alternative interventional treatments such as D-TACE, TARE, or combining of other therapies like radiotherapy and ablation therapy, are suggested to potentially enhance treatment response and improve OS.

In recent years, several studies have focused on the efficacy of TACE or HAIC combined with TKIs and ICIs. However, as the clinical practice of HAIC deepened, it became apparent that simple HAIC presents limitations in treating liver tumors, including multiple tumors located in different liver lobes or supplied by multiple blood vessels, large tumors, and arteriovenous fistulas. When HAIC alone is used to treat these patients, positioning the catheter satisfactorily poses a challenge. Consequently, the advantages of HAIC cannot be fully realized. In our study, for tumors with multiple blood supply arteries including the superior mesenteric artery, diaphragmatic artery, and left gastric artery—excluding the left and right hepatic arteries—we performed embolization on the non-main blood supply branches prior to catheter placement and subsequently positioned the catheters in the main blood supply vessels for chemotherapy drug infusion.

In this study, uHCC patients receiving TACE-HAIC combined with TKIs and PD-1 inhibitors achieved a median PFS of 14 months and a median OS of 26.2 months. Compared to previous clinical studies, patients have better survival benefits [21–24]. However, this study's ORR (41.0%) and DCR (55.7%) were lower than those reported in previous studies, potentially due to the advanced tumor stages of participants, especially those with a larger average tumor diameter (95.38 ± 38.12 mm) and a high prevalence of BCLC stage C (83 patients,

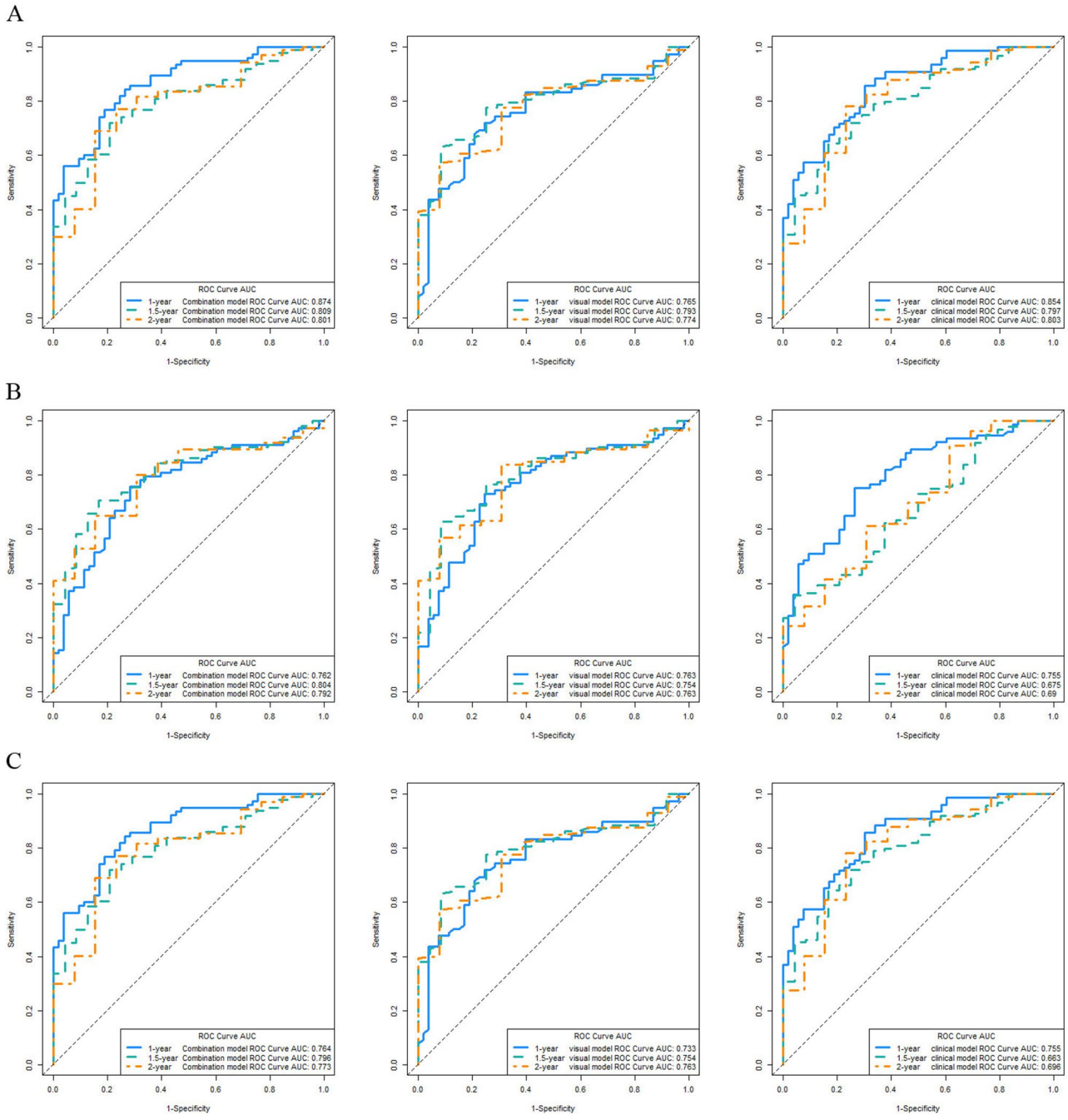

Fig. 5 The ROC curves of the abovementioned three models

68.0%). Interestingly, our findings closely aligned with a similar retrospective study that utilized TACE in conjunction with HAIC, molecular targeted drugs, and immunotherapy. In that study, the combination therapy group demonstrated a significant advantage in PFS compared to the control group receiving TACE alone, with PFS of 14.8 months versus 2.3 months ($P < 0.001$), respectively. Unfortunately, the median OS was not reached in this study [5]. This suggests that this quadruple therapy approach can significantly enhance the overall prognosis for patients with unresectable hepatocellular carcinoma, particularly for those with portal vein tumor thrombosis. Nevertheless, a subset of patients may not benefit from this combination treatment, making the prediction of such differences before undergoing combination therapy particularly crucial.

The integration of artificial intelligence to combine radiomics features with clinical features for constructing clinical-radiomic models has been widely applied in predicting treatment outcomes, demonstrating good

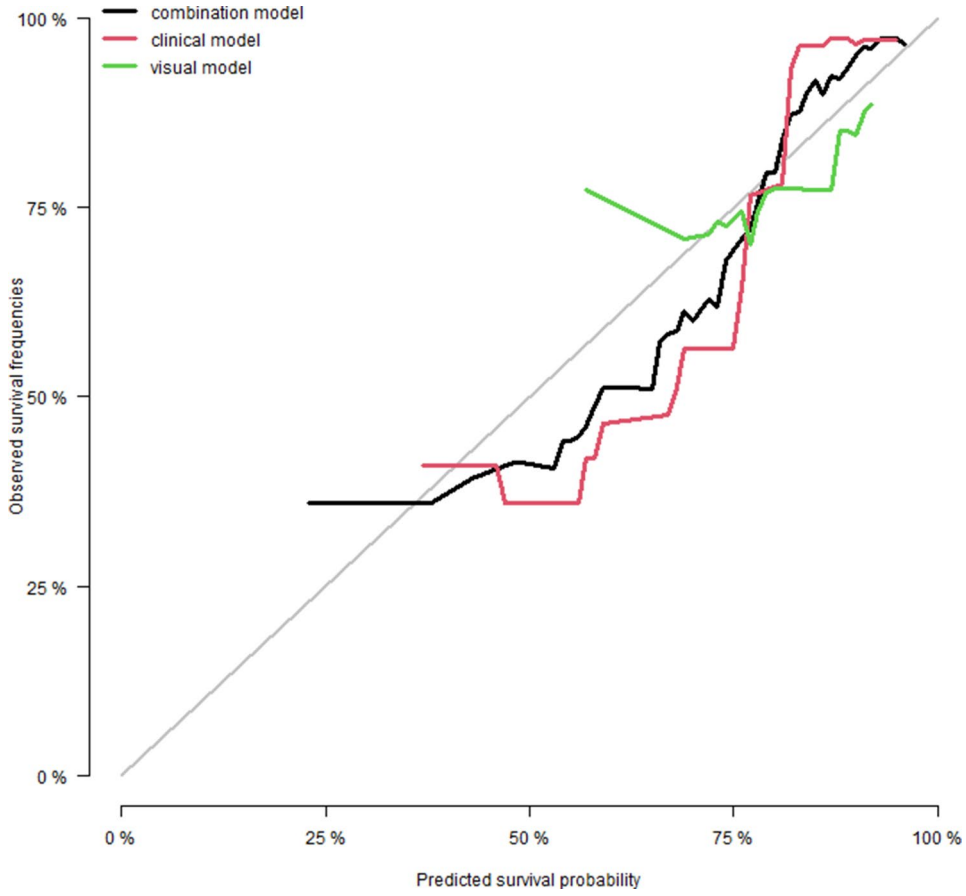

Fig. 6 The calibration curves of the abovementioned three models

predictive performance. In our study, we employed deep learning technology to build a multimodal model that achieved high predictive performance, with an AUC of 0.97 and accuracy of 0.91. Such predictive capability was similar to the results obtained in several previous studies using machine learning or deep learning-based C-R models [14, 25, 26]. Compared to these studies, our model was developed on a more limited dataset. We achieved comparable predictive performance by further enhancing the ResNet50 algorithm. Specifically, an additional MLP (Multilayer Perceptron) layer was incorporated, ensuring comprehensive data coverage and efficient model training. This modification allowed for the effective selection of key image features, thereby reducing the computational burden on subsequent classification layers. By employing L2 regularization and Dropout within the MLP, overfitting issues associated with smaller datasets were effectively mitigated. This integrated approach facilitated the construction of a more robust predictive model. Through this model, we can explore the interactions between imaging data and clinical characteristics, enabling more comprehensive and precise disease assessment.

Most studies use univariate and multivariate Cox regression analyses to select variables and construct models based on clinical and radiomic characteristics. We constructed clinical, radiomic, and clinical-radiomic combined prediction models, and found that the clinical-radiomic model demonstrated superior predictive capabilities, similar to previous studies [15, 27]. The clinical features included in clinical-radiomic model were elevated levels of AFP, type VP4 portal vein tumor thrombus, larger tumor diameter, and the presence of tumor capsule. This slightly differs from previous studies [14, 27, 28], potentially due to the limited sample size in our study. Nonetheless, we observed that certain clinical features not included in the combined model, such as the number of tumors and the presence of extrahepatic metastasis, could significantly impact prognosis.

This study had some limitations. First, it was a single-center retrospective study with a small sample size, potentially reducing the reliability of the model. Therefore, to develop a more accurate predictive model, a prospective, multicenter study with a larger sample size is necessary. Second, due to the short follow-up period, obtaining final survival-related data for most patients was not feasible, preventing the construction of OS-related

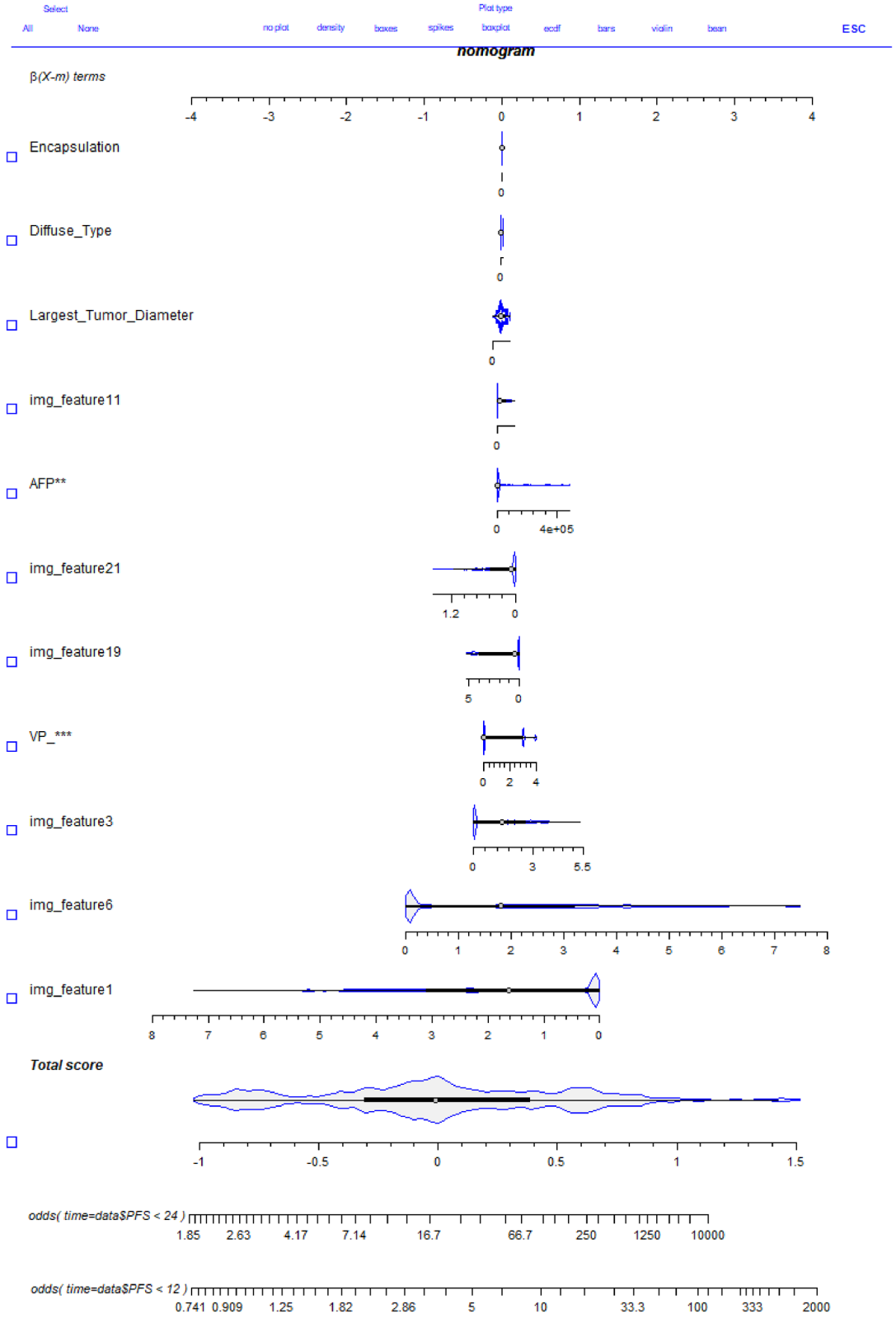

Fig. 7 The nomogram for predicting PFS following combination therapy

prediction models; therefore, constructing OS-related prediction models was not possible. Further follow-up could address this limitation. Third, in this study, the frequency of receiving TACE-HAIC combination therapy was inconsistent, which may affect the treatment response and survival time of patients. Future research will aim to analyze the correlation between various frequencies of combination therapy and their efficacy.

Conclusion

The study developed and validated a joint model of imaging omics and clinical data based on deep learning, designed to serve as a tool for predicting treatment response and PFS in patients receiving TACE-HAIC combined with TKIs and PD-1 inhibitor combination therapy. It offers potential to provide critical evidence for clinical doctors in identifying patients who may benefit from combination therapy.

Abbreviations

CT	Computed tomography
HCC	Hepatocellular carcinoma
TACE	Transarterial chemoembolization
HAIC	Hepatic arterial infusion chemotherapy
TKIs	Tyrosine kinase inhibitors
ResNet	Residual convolutional neural network
ROC	Receiver operating characteristic
AUC	Area under the curve
ORR	Objective response rate
DCR	Disease control rate
PFS	Progression-free survival
OS	Overall survival
BCLC	Barcelona Clinic Liver Cancer
VEGF	Vascular endothelial growth factor
ECOG	Eastern Cancer Collaborative Group
CNLC staging	China liver cancer staging
mRECIST	Modified Response Evaluation Criteria in Solid Tumors
OR	Objective response
NR	No response
CR	Complete response
PR	Partial response
SD	Disease stability
PD	Disease progression
TRAEs	Treatment-Related Adverse Events
CTCAE	Common Terminology Criteria for Adverse Events
ROI	Region of interest
CNN	Convolutional neural network
MLP	Multilayer perceptron

Supplementary Information

The online version contains supplementary material available at https://doi.org/10.1186/s12876-024-03555-7.

Supplementary Material 1

Supplementary Material 2

Supplementary Material 3

Supplementary Material 4

Acknowledgements

Not applicable.

Author contributions

Liu RB and Yin LN initiated and designed the study; Li W, Li SJ and Hou XB acquired the data; Yin LN and Li W performed the analyses and interpreted the data; Yin LN drafted the paper; Yin LN and Liu RB revised this manuscript; all authors have read and approve the final manuscript.

Funding

Not applicable.

Data availability

The data sets used during the study are available from the corresponding author on reasonable request.

Declarations

Ethics approval and consent to participate

Approval for the study was obtained from the Ethics Committee of Harbin Medical University Cancer Hospital (Ethics number: 2023-281-IIT). Written informed consent was not required due to the retrospective nature of the study, and the need for consent to participate was also waived by the ethics committee.

Consent for publication

Not Applicable.

Competing interests

The authors declare no competing interests.

Author details

[1]Department of Interventional Radiology, Harbin Medical University Cancer Hospital, No. 150 Haping Road, Nangang District, Harbin, Heilongjiang Province 150081, China
[2]Department of Interventional Radiology, Affiliated Fourth Hospital of Harbin Medical University, 37 Yiyuan Street, Nangang District, Harbin, Heilongjiang Province 150001, China

Received: 31 July 2024 / Accepted: 9 December 2024
Published online: 21 January 2025

References

1. Tao Y, Wang J, Xu X. Emerging and innovative theranostic approaches for mesoporous silica nanoparticles in Hepatocellular Carcinoma: current status and advances. Front Bioeng Biotechnol. 2020;8:184.
2. Villanueva A. Hepatocellular Carcinoma. N Engl J Med. 2019;380:1450–62.
3. Craig AJ, von Felden J, Garcia-Lezana T, Sarcognato S, Villanueva A. Tumour evolution in hepatocellular carcinoma. Nat Rev Gastroenterol Hepatol. 2020;17:139–52.
4. Park J, Chen M, Colombo M, et al. Global patterns of hepatocellular carcinoma management from diagnosis to death: the BRIDGE Study. Liver Int. 2015;35:2155–66.
5. Yuan Y, He W, Yang Z, et al. TACE-HAIC combined with targeted therapy and immunotherapy versus TACE alone for hepatocellular carcinoma with portal vein tumour thrombus: a propensity score matching study. Int J Surg. 2023;109:1222–30.
6. Li B, Qiu J, Zheng Y, et al. Conversion to Resectability using Transarterial Chemoembolization Combined with hepatic arterial infusion chemotherapy for initially unresectable Hepatocellular Carcinoma. Ann Surg Open. 2021;2:e057.
7. Sergio A, Cristofori C, Cardin R, et al. Transcatheter arterial chemoembolization (TACE) in hepatocellular carcinoma (HCC): the role of angiogenesis and invasiveness. Official J Am Coll Gastroenterology| ACG. 2008;103:914–21.
8. Song B, Chung Y, Kim JA, et al. Association between insulin-like growth factor-2 and metastases after transcatheter arterial chemoembolization in patients with hepatocellular carcinoma: a prospective study. Cancer. 2001;91:2386–93.
9. Xiong ZP, Yang SR, Liang ZY et al. Association between vascular endothelial growth factor and metastasis after transcatheter arterial chemoembolization in patients with hepatocellular carcinoma. Hepatobiliary & Pancreatic Diseases International: HBPD INT. 2004;3:386 – 90.

10. Kadalayil L, Benini R, Pallan L, et al. A simple prognostic scoring system for patients receiving transarterial embolisation for hepatocellular cancer. Ann Oncol. 2013;24:2565–70.
11. Hucke F, Pinter M, Graziadei I, et al. How to STATE suitability and START transarterial chemoembolization in patients with intermediate stage hepatocellular carcinoma. J Hepatol. 2014;61:1287–96.
12. Sieghart W, Hucke F, Pinter M, et al. The ART of decision making: retreatment with transarterial chemoembolization in patients with hepatocellular carcinoma. Hepatology. 2013;57:2261–73.
13. Zhang H, Luo K, Deng R, Li S, Duan S. Deep learning-based CT imaging for the diagnosis of Liver Tumor. Comput Intell Neurosci. 2022;2022:3045370.
14. Chen M, Cao J, Hu J, et al. Clinical-radiomic analysis for pretreatment prediction of objective response to first transarterial chemoembolization in hepatocellular carcinoma. Liver Cancer. 2021;10:38–51.
15. Liu P, Zhu H, Zhu H, et al. Predicting survival for hepatic arterial infusion chemotherapy of unresectable colorectal liver metastases: Radiomics analysis of pretreatment computed tomography. J Translational Intern Med. 2022;10:56–64.
16. Wang F, Chen Q, Zhang Y et al. CT-Based Radiomics for the recurrence prediction of hepatocellular carcinoma after surgical resection. Journal of Hepatocellular Carcinoma. Published online 2022:453 – 65.
17. Mu W, Jiang L, Shi Y, et al. Non-invasive measurement of PD-L1 status and prediction of immunotherapy response using deep learning of PET/CT images. J Immunother Cancer. 2021;9:6.
18. Mu W, Jiang L, Zhang J, et al. Non-invasive decision support for NSCLC treatment using PET/CT radiomics. Nat Commun. 2020;11:5228.
19. Yang L, Xu P, Li M, et al. PET/CT radiomic features: a potential biomarker for EGFR mutation status and survival outcome prediction in NSCLC patients treated with TKIs. Front Oncol. 2022;12:894323.
20. Zhou J, Sun H, Wang Z, et al. Guidelines for the diagnosis and treatment of primary Liver Cancer (2022 Edition). Liver Cancer. 2023;12:405–44.
21. Finn RS, Qin S, Ikeda M, et al. Atezolizumab plus Bevacizumab in unresectable hepatocellular carcinoma. N Engl J Med. 2020;382:1894–905.
22. Qin S, Chan SL, Gu S, et al. Camrelizumab plus Rivoceranib versus Sorafenib as first-line therapy for unresectable hepatocellular carcinoma (CARES-310): a randomised, open-label, international phase 3 study. Lancet. 2023;402:1133–46.
23. Li QJ, He MK, Chen HW, et al. Hepatic arterial infusion of oxaliplatin, fluorouracil, and leucovorin versus transarterial chemoembolization for large hepatocellular carcinoma: a randomized phase III trial. J Clin Oncol. 2022;40:150–60.
24. Yuan Y, He W, Yang Z, et al. TACE-HAIC combined with targeted therapy and immunotherapy versus TACE alone for hepatocellular carcinoma with portal vein tumour thrombus: a propensity score matching study[J]. Int J Surg. 2023;109:1222–30.
25. iu XK, He XF. Development of a computed tomography-based radiomics nomogram for prediction of transarterial chemoembolization refractoriness in hepatocellular carcinoma. World J Gastroenterol. 2021;27:189.
26. Liu QP, Yang KL, Xu X, Liu XS, Qu JR, Zhang YD. Radiomics analysis of pretreatment MRI in predicting tumor response and outcome in hepatocellular carcinoma with transarterial chemoembolization: a two-center collaborative study. Abdom Radiol Published Online 2022:1–13.
27. Yang Y, Zhou Y, Zhou C, Ma X. Deep learning radiomics based on contrast enhanced computed tomography predicts microvascular invasion and survival outcome in early stage hepatocellular carcinoma. Eur J Surg Oncol. 2022;48:1068–77.
28. Kong C, Zhao Z, Chen W, et al. Prediction of tumor response via a pretreatment MRI radiomics-based nomogram in HCC treated with TACE. Eur Radiol. 2021;31:7500–11.

Publisher's note